Borophene: A Piezocatalyst

Aditi Sharma[1], Upasana Bhardwaj[1], Maya Marinova[2], Antonio Da Costa[3], Anthony Ferri[3], Sebastien Royer[3*], Jérémy Dhainaut[3*] & Himmat Singh Kushwaha[1,*]

[1]Materials Research Centre, Malaviya National Institute of Technology Jaipur (MNITJ), India

[2]Université de Lille, CNRS, INRA, Centrale Lille, Université Artois, FR 2638 – IMEC – Institut Michel-Eugène Chevreul, 59000 Lille, France

[3]Univ. Lille, CNRS, Centrale Lille, Univ. Artois, UMR 8181 - UCCS - Unité de Catalyse et Chimie du Solide, F-59000 Lille, France

[*]Corresponding Authors

E-mail: himmatsingh.mrc@mnit.ac.in,
sebastien.royer@univ-lille.fr,
jeremy.dhainaut@univ-lille.fr

Graphical Abstract

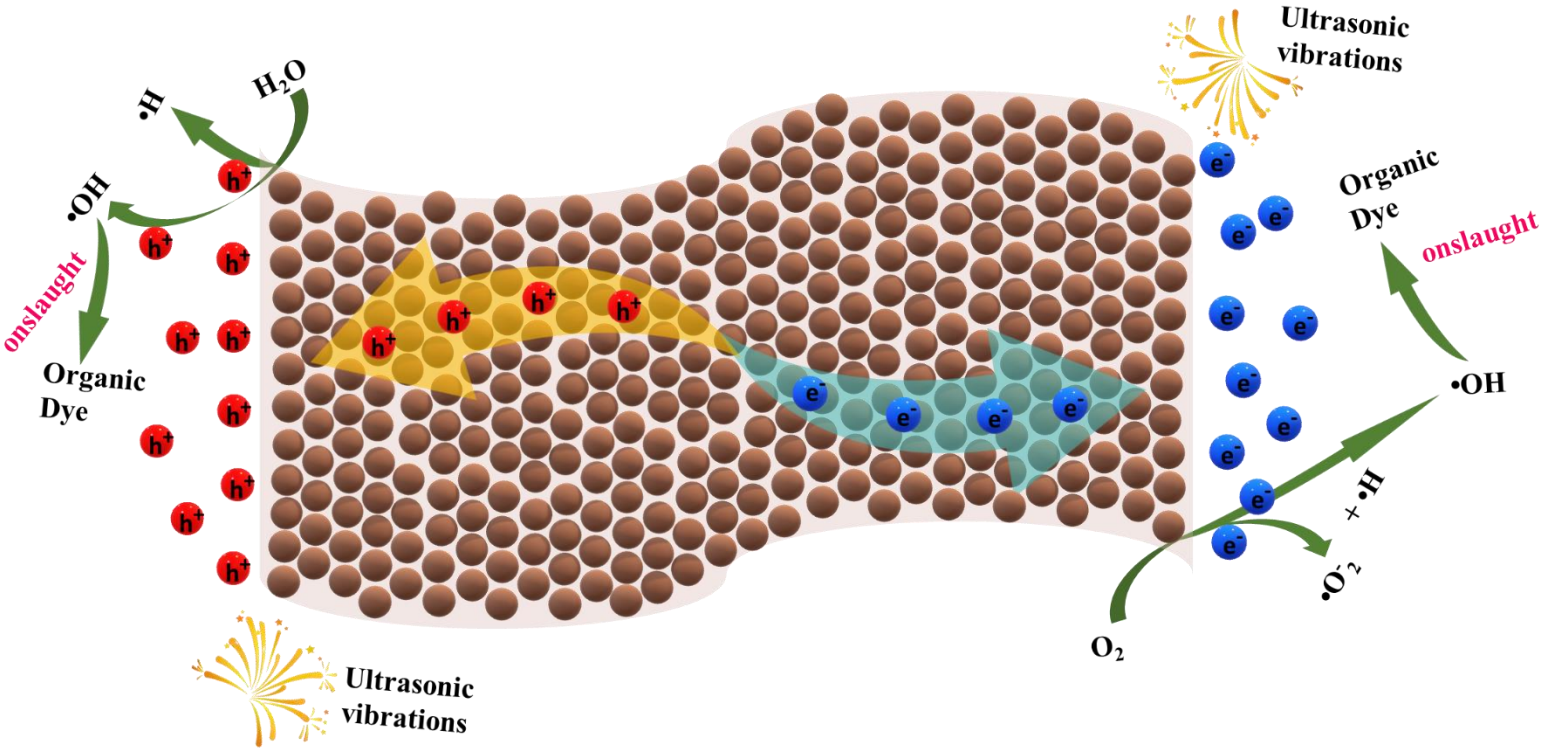

Abstract

Borophene was successfully synthesized by modifying the Hummer's approach. Under the influence of ultrasonic vibrations, two-dimensional borophene sheets exhibit exceptional piezocatalytic activity, as exemplified by the decomposition of highly stable organic pollutants in water. After only 1 minute of exposure, the piezocatalytic activity of borophene sheets converted up to 99 percent of the initial molecules of rose bengal dye (50 mg/L) at room temperature, neutral pH. The principal active oxidant species have been identified as superoxide ($\bullet O_2^-$) and hydroxyl radicals ($\bullet OH$) formed from H_2O and dissolved O_2. The induction of polarized electric charges has also been measured during the process. Further elucidation of the piezocatalytic mechanism suggests that the piezocatalytic efficiency can be related to the piezoelectric effect generating electric charges to increase charge transfer during chemical redox reactions. Our research provides new insights into the preparation of borophene and its use as piezo catalysts for environmental catalysis.

1. Introduction

Water contamination is one of humanity's most significant environmental problems. The discharge of high-soluble and chemically stable contaminants into effluents is the main cause of water contamination. Recently, piezoelectric polarization has attracted a growing amount of attention in the field of water purification[1] as it can be applied to increase the separation of photogenerated charge carriers for the enhancement of photocatalytic efficiency[2,3]. Furthermore, it can operate as a sole driving force to initiate the catalytic reaction[4], a process known as piezocatalysis.

Piezocatalysis is an emerging technique based on the piezoelectric effect of materials lacking a center of symmetry. Such materials deform themselves under the effect of mechanical vibrations, causing spontaneous polarization. Then, the free charge carriers inside the materials will be separated through the induced piezo potential and could migrate to the surface to further engage in redox reactions[1,5]. Similar to electrocatalysts and photocatalysts, piezocatalysts may not only directly employ mechanical energy to drive reactions such as advanced oxidation processes, but they could also be used as a mean to store mechanical energy in green power carriers like hydrogen. The piezoelectricity produced by mechanical distortion in piezoelectric materials has found widespread application in sensing, actuators, and high-voltage generators[6]. Most known piezoelectric devices are comprised of bulk materials like ceramics and single crystals. The application of nanosized piezoelectric materials in energy conversion is newer[7]. Consequently, piezocatalysis is seen as a new powerful technique for addressing environmental and energy issues[8]. Among numerous reported piezocatalysts ZnO[9,10], $BaTiO_3$[11], $KNbO_3$[12], $NaNbO_3$[13,14], and CdS[15] have been extensively utilized for environmental decontamination. Unfortunately, such metal oxide and sulfide piezoelectric materials rapidly deteriorate (< 1 h in reaction).

Two-dimensional materials, have garnered a great deal of interest due to their high surface-to-volume ratio and exceptional electronic properties, which grant them with a greater potential for various applications such as energy storage, sensing, electronics, aerospace structures than their bulk form[16]. In 2014, it was discovered for the very first time that single- as well as few-layered MoS_2 exhibit substantial piezoelectric properties[17]. After the development of 2D materials such as graphene[18], silicene[19], hexagonal boron nitride[20], stanine, aluminum nitride sheet, phosphorene[21], arsenene, molybdenum disulfide, and antimonene, 2D boron sheets known as borophene was unveiled[22]. Borophene has rich architectural diversity, exhibiting unique physical and chemical

properties including- in-plane anisotropy, ultrahigh thermal conductance, superconductivity, high carrier mobility, presence of dirac fermions, and optical transparency[23–26]. Boron-related 2D compounds are distinguished from other 2D materials by their polymorphism[27–29], i.e., the capacity of boron to create multicenter bonding arrangements enabling the formation of a large variety of stable 2D phases. Initially, borophene was synthesized by CVD on a metal substrate (silver, copper *etc*) under high vacuum. As 2D materials offer unique features of interest of surface induced reactions[30], borophene has lately been reported to display strong electrocatalytic activity for NH_3 production from N_2 in neutral environments[31]. Current theoretical and experimental research has demonstrated that α-phase molybdenum diboride (-MoB_2) containing borophene subunits devoid of noble metals possesses superefficient electrocatalytic characteristics for the hydrogen evolution reaction[32]. These results have directed our interest to further investigate borophene as a piezocatalyst for advanced oxidation processes.

Herein, we present the synthesis of borophene sheets through the modified Hummer's method starting from borophene oxide . The resulting two-dimensional material is easily deformable, and its flat surface gives a large area for capturing mechanical energy. Under ultrasonication, these nanosheets readily degrade organic pollutants such as organic dyes in water. By monitoring the reactive radicals produced during the piezocatalytic process, a degradation mechanism of organic dyes involving superoxide ($\bullet O_2^-$) and hydroxyl (•OH) oxidant radicals is proposed.

2. Experimental Section:

2.1 Synthesis of borophene

Borophene Oxide was synthesized by using a modified Hummer's method[33,34]. [caution: violent reaction, with possible projection, can occurs – reaction should be performed under fumehood with personal protections]. Initially, pure boron powder and potassium permanganate ($KMnO_4$) were

mixed in a proportion of 1:6 and ground for 10 minutes. Simultaneously, an acidic mixture was prepared by mixing ortho-phosphoric acid (H_3PO_4) and sulfuric acid (H_2SO_4) in a ratio of 1:9. To control the reaction exothermicity, a precooling procedure was followed by cooling these two mixtures below 5 °C for six hours. When the Boron + $KMnO_4$ mixture was poured into the acidic mixture, it immediately ignited and caught flame, eventually turning into dense brown smoke due to an exothermic reaction as shown in Fig. S1 and the residual mixture were combined and ultrasonicated for 24 hours at 65^oC to produce borophene oxide sheets. After, 200 mL of distilled water were added to quench the reaction, and the mixture was sonicated for another 2 hours. After the completion of the reaction, the product was washed with distilled water (3 times), ethanol (2 times), and 1M HCl (17.5%, 2 times) and dried at 65 ^oC for 12 hours[35,36].

2.2 Piezocatalytic experiments

The Piezocatalytic activity of borophene was evaluated by monitoring the degradation of selected dyes: rose Bengal (50 mg/L, anionic dye), methylene blue (10 mg/L, cationic dye), and mixture of dye (rose Bengal (50 mg/L), methylene blue (10 mg/L), rhodamine B (10 mg/L), and methyl orange (10 mg/L)). borophene was added to the 40 mL of dye solution to reach the 0.5 mg/mL. Before conducting piezocatalysis, the adsorption-desorption equilibrium between the catalyst and dye solution was achieved by keeping it in a dark environment for 1 hour. The piezocatalysis experiments were carried out after this step. Upon exposure to ultrasonic vibrations, 2 mL aliquots were collected every minute for the evaluation of the dye concentration by UV-visible spectrophotometry[37].

2.3 Reusability test for borophene

During the piezocatalytic degradation of the organic dye methylene blue, the utilized borophene nanosheets were effectively recovered by centrifugation, rinsed three to four times with distilled

water, and then dehydrated for two hours in a vacuum oven at 60 degrees Celsius. This was done to ensure that the nanosheets were free of any moisture. For the purpose of investigating the repeatability of borophene nanosheets, this procedure was carried out five times[9,38].

3. Material Characterization

A Bruker D8 Advanced AXS diffractometer was used to acquire powder X-ray diffraction (PXRD) patterns. A monochromatic irradiation source (λ= 1.5418 Å) and 40 kV and 30 mA were used to run the diffractometer. The X-ray diffractograms were recorded using a 1 s step time and a 0.02 step size. High angle annular dark field (HAADF) photography and scanning transmission electron microscopy (STEM) were performed with a Titan Themis FEI FEG TEM/STEM system operating at 300 kV. The samples was directly observed as a powder or as thin foil (50 nm) fabricated using an ultramicrotome (Leica Ultracut S) after dispersing the material in an epoxy resin and curing at 50 °C For the chemical composition analysis. High-resolution X-ray Photoelectron Spectra (XPS) were acquired using a Kratos Analytical AXIS UltraDLD spectrometer outfitted with a monochromatic Al Kα X-ray laser (1486.6 eV) and a continuous passage energy of 20 eV. Casa XPS was used for spectral decomposition and quantification. A dual beam UV-Vis NIR spectrometer was used to test the material's optical characteristics (LAMBDA 750-Perkin Elmer). Using an IRIX STR 500 Raman spectrometer, Raman spectroscopy was used to assess the crystallographic orientation of the produced borophene. The results were collected using a 532 nm Ar ion laser at room temperature (about 1 mW, 50 objective). Fourier Transformation infrared spectroscopy (FT-IR) was used to identify the chemical components and bonds. To identify the lateral size and number of sheets of the borophene sheets, atomic force microscopy (AFM, Bruker) was used. The piezoelectricity was locally probed by using the piezoresponse (PFM) mode of the AFM technique by means of an MFP-3D (Asylum Research/Oxford Instruments, USA)

microscope under environment conditions. The dual AC resonance tracking (DART) method[39] of the PFM was used for both imaging and spectroscopy modes, and remnant PFM signal (at zero bias) was preferentially recorded when measuring piezoresponse loops in order to promote electromechanical response at the expense of the electrostatic contribution[40]. The generation of hydroxyl radicals in the excitation range of 200-800 nm was measured using a fluorescence spectrometer (LS 55 (Perkin Elmer)). A digital scanning oscilloscope was used to measure the piezoelectric voltage production (DSO).

4. Result and Discussion

The XRD pattern of the synthesized borophene sheets is depicted in Fig. 1a, and it matches well with the β–rhombohedral crystalline structure[41] of boron (ICDD card no 11-0618). Hence, to confirm the formation of borophene sheets, their raman spectrum is depicted in Fig. 1b. The improved Hummer's process produced borophene sheets with distinct Raman peaks at 676.8 cm^{-1}, 880 cm^{-1}, 1126.94 cm^{-1}, 1152.26 cm^{-1}, 1264.4 cm^{-1} and 1290.88 cm^{-1}. Borophene, unlike graphene, is anisotropic; as a result, its symmetry axes are not identical, resulting in multiple distinctive peaks[35]. Fig. 1c depicts the FT-IR spectrum of as-prepared borophene sheets. It is observed that there are only two visible peaks in the spectrum which correspond to B-O and B-B bands occurring at 1050 cm^{-1}, 890 cm^{-1}, respectively[42]. High resolution XPS, as shown in Fig. 1d was further applied to evaluate the surface composition of borophene. As-synthesized borophene display three peaks in B 1s spectrum centered at 192.5, 189.1, and 187.7 eV, showing that B created three types of bonding structures. The principal component related to a B–B bond at 187.7 eV is comparable with the previously reported values for bulk B (187.3-187.9 eV)[43], while the peak attributed to the B–O bond in a boron-rich oxide, is located at 189.1 eV. The 192.5 eV signal

appears to be related to the production of B_2O_3, indicating that borophene may be partially oxidized due to its large contact area[44].

High resolution HAADF pictures of the prepared borophene are displayed on Fig. 2. Fig. 2a-b clearly shows that the prepared borophene has the expected honeycomb-like structure. Moreover, Fig. 2b attests the crystalline nature of the borophene nanosheets[45,46]. Fig. 2c allows determining an interplanar distance of about 0.32 nm. Fig. 2d-e shows atomic force microscopy (AFM) images depicting that the thickness of borophene stacked nanosheets ranges from 1 to 2 nm. The stacking of borophene nanosheets may be appreciated from Fig. 2e, while its lateral dimensions several 100 nm are clearly observed in Fig. 2d.

A PFM approach was used to probe the piezoelectric properties of borophene nanosheets at the nanoscale. When a AC driving voltage is applied to the sample via the AFM tip, the ensuing mechanical deformation of the material is induced due to the converse piezoelectric effect[47]. The as-grown out-of-plane (OP) and in-plane (IP) amplitude piezoresponse pattern measured over the surface of the borophene sample is presented on Fig. 3b and c respectively, simultaneously recorded with the topography in Fig. 3a. Strong piezoelectric response is detected along both OP and IP direction, as revealed by the bright contrasts. By superimposing a continuous DC bias voltage (voltage pulse bias ramps from -10 V to +10 V) on the intermittent AC signal, amplitude piezoresponse loops can be recorded. As seen in Fig. 3d, a well-defined butterfly-shaped loop is obtained, evidencing clear piezoelectric behavior in borophene[48,49], in agreement with amplitude PFM pattern in Fig. 3b.As a remark, the poor quality of the AFM topographic image presented on Fig. 3a is mainly due to the contact mode required for recording piezoresponse signal.

Fig. 4a shows digital scanning oscilloscope (DSO) measurements of the open circuit voltage response of mechanically stressed borophene sheets. Under bending conditions, the maximum

voltage reaches up to 0.078 V, and it reaches 0.18 V when pressure was exerted by manual tapping. When pressure is imposed onto the borophene sheets, the induced piezo potential generates positive impulses, and when pressure is removed from the borophene sheets, the induced piezo potential generates negative impulses. The piezoelectric effect was not observed in the absence of vibrations, implying that no pressure was applied to or removed from the borophene sheets[37,50]. Fig. 4b shows the piezo current response for the borophene sheets. It has good charge separation efficiency and high electron mobility.

Borophene was applied to the degradation of organic pollutants, and the piezocatalytic results are depicted in Fig. 5a-c. Within 1 minute of ultrasonic vibrations, the absorbance peak of rose bengal at 559 nm disappears, indicating effective dye degradation (Fig. 5a). In the case of methylene blue, the absorbance peak at 668 nm decreases significantly from 4 minutes of ultrasonic vibrations (Fig. 5b). The difference in degradation efficiencies could be explained by the existence of aromatic rings and the amount and type of substituents on the ring (such as electron giving or electron-withdrawing groups), which affect adsorption and subsequently the rate of degradation[51]. Fig. 5c shows the degradation of a mixture of dyes (rhodamine b, methylene blue, methyl orange, and rose Bengal) following up to 6 minutes of exposure time under ultrasonic vibrations. It has been showed that 92% of all dye molecules were readily deteriorated at room temperature and without addition of an oxidant as typically done in photocatalysis (H_2O_2, persulfates). The relating decomposition ratios are summed up in Fig. 5d. Methylene blue, rose Bengal, and dye mixtures were degraded up to 97%, 99%, and 92% after 6 minutes. Fig. 5e depicts the degradation efficiency curve, which was computed by subtracting the starting concentration from the concentration obtained after treatment, and it was observed that no degradation occurs when ultrasonic vibrations are applied to organic dyes in the absence of borophene nanosheets. The corresponding rate constant (ln kt=

C/C_0) was determined by fitting the empirical observations to the pseudo-first order kinetic rate equation ($\ln kt = C/C_0$), as shown in Fig. 5f. The results show that borophene has a robust catalytic effect under mechanical vibrations, with high breakdown performance and rate constant. Under ultrasonication, the degradation impact of methylene blue ($k = 0.449\ min^{-1}$) is 1.35 times greater than that of a dye combination ($k = 0.606\ min^{-1}$). Based on the observations, borophene may be utilized for both cationic and anionic dyes. In addition, the recyclability of borophene for degrading MB in the presence of ultrasonic vibration was examined. After five recycling operations, the degradation efficiency shows no discernible changes, but after five cycles the degradation efficiency reduced slightly, confirming the robustness of piezo-catalysts for long-term durability (Fig. S2-a). The structural stability of borophene nanosheets also provides solid proofs that the degradation of methylene blue is caused by the piezo-catalysis effect of borophene nanosheets, rather than any chemical reaction between borophene and organic dye (Fig. S2-b). As shown in figure 2 a novel peak emerges at around 28˚, characterizing a slight formation of boron oxide after the reaction. The utilized borophene has a B 1s spectrum with three peaks centered at 192.2, 189.0, and 187.6 eV (Fig. S2-c). Table S1 represents the comparison between different piezocatalytic systems, highlighting the superior performances of borophene.

Throughout the piezocatalytic process, fluorescence spectroscopy was employed to detect the formation of hydroxyl radicals (•OH) as •OH radicals rapidly interact with terephthalic acid to form 2-hydroxyterephthalic acid, a highly fluorescent drug with a signal at 425 nm under 315 nm excitation[67]. As observed in Fig. 6a, borophene under ultrasonic irradiation produces a consequent amount of hydroxyl radicals which are one of the main active species in liquid-phase advanced oxidation processes.. Furthermore, the degradation of nitro blue tetrazolium chloride (NBT, 4.9×10^{-5} M), which is a scavenger for super oxide radicals ($\bullet O_2^-$), was carried out under the same

conditions as dyes degradation[8]. As illustrated in Fig. 6b, its rapid degradation shows consequent formation of $\bullet O_2^-$.

Based on the above findings, a potential catalytic mechanism interpretation is proposed in Fig. 7(a-d). In piezocatalysis, the mechanical energy like ultrasonic vibrations can spontaneously energize electrons from the valence band (V.B) to the conduction band (C.B) as implosion of cavitation bubbles can briefly generate high pressures (10^8 Pa) and local hotspot (~5000 K) at the catalyst/water interface, which gives ample energy for electron excitation[54,55]. Moreover, the recombination of thus-generated electrons (e^-) and holes (h^+) is largely reduced due to the piezoelectric polarization effect. Hence, they can react with water in order to produce free hydroxyl radicals (•OH), which further oxidize the dye molecules as mentioned in equations (1-2)[56,57,9].

$$\text{Ultrasonic vibrations} + H_2O \longrightarrow H^+ + \bullet OH \qquad (1)$$

$$\bullet OH + \text{dye molecules} \longrightarrow \text{degraded products} \qquad (2)$$

As illustrated in Fig. 7a, bound charges on the piezoelectric material's surface are initially in equilibrium with screening charges, resulting in an electrically neutral material[58]. When the mechanical stress is applied to the borophene sheets through ultrasonic vibrations, a piezoelectric polarization is induced inside the material which will further attract the free e^- and h^+ within the borophene sheets in opposite directions toward the materials surface, as shown in Fig. 7a. This induced piezoelectric potential concurrently tilts the C.B and V.B. As a result, higher the piezoelectric potential, the more easily and rapidly e^- and h^+ react with water and dissolved oxygen to form reactive oxygen species[59,53]. When the mechanical stress is imposed at its maximum level, the polarized charges will be minimized. The additional screening charges will continue to be released until the material attains new electrostatic balance[60], as shown in Fig. 7c. When the applied stress is released, then the newly formed electrostatic equilibria will break again, leading

to reverse charge transfer and new redox reactions, as shown in Fig. 7d. In a similar manner to forward loading, the redox reactions at the solid-liquid interface won't last long due to the depletion of the surface charge. The free charges (e^- and h^+) that were spent by redox reactions can be produced again thermally by the mechanical energy (ultrasonic vibrations), producing the apparent piezocatalytic effect.

The possible reactions that occur in the degradation mechanism is depicted in equations (3-6)

$$\text{Borophene sheets + mechanical stress} \longrightarrow \text{borophene } (e^- + h^+) \quad (3)$$

$$O_2 + e^- \longrightarrow \bullet O_2^- \quad (4)$$

$$H_2O + h^+ \longrightarrow \bullet OH \quad (5)$$

$$\bullet O_2^- / \bullet OH + \text{pollutants} \longrightarrow \text{degradation products} \quad (6)$$

Conclusion

This paper described the synthesis of borophene nanosheets, as well as their thorough characterization and application to piezocatalysis. The formation of a piezo-potential within the borophene nanosheets under the mechanical stress was measured to be ~ 0.2 V. Utilizing ultrasonic vibration energy, the piezocatalytic ability of borophene nanosheets to decompose a mixture of organic dyes has been investigated. It demonstrates that borophene nanosheets, as a novel piezocatalyst, display increased piezocatalytic breakdown of dyes. In the piezocatalytic mechanism, the hydroxyl (•OH) and superoxide ($\bullet O_2^-$) radicals are the primary active species that are produced from polarized electric charges. Our work will encourage additional research in the fields of piezocatalysis, piezocatalytic performance, and piezocatalytic mechanism.

Acknowledgement

The researchers would like to acknowledge the Water Technology Initiative (WTI) scheme, Department of Science and Technology (DST), New Delhi under INSPIRE faculty award-2018

(MS-146), India, and the French Government (Eiffel Excellence Scholarship 2022) for providing the financial support for this research work. The CNRS, the Chevreul Institute (FR 2638), the Ministère de l'Enseignement Supérieur et de la Recherche, the Région Hauts-de-France, the FEDER, and the MEL are acknowledged for supporting this work. Région Hauts-de-France and Fonds Européen de Développement Régional (FEDER) are gratefully acknowledged for funding the MFP-3D microscope under Program "Chemistry and Materials for a Sustainable Growth". Dr. Pardis Simon is acknowledged for XPS measurements

References

1. Liang, Z., Yan, C. F., Rtimi, S. & Bandara, J. Piezoelectric materials for catalytic/photocatalytic removal of pollutants: Recent advances and outlook. *Appl. Catal. B Environ.* **241**, 256–269 (2019).
2. Yu, Y. & Wang, X. Piezotronics in Photo-Electrochemistry. *Adv. Mater.* **30**, 1–16 (2018).
3. Xue, X. *et al.* Piezo-potential enhanced photocatalytic degradation of organic dye using ZnO nanowires. *Nano Energy* **13**, 414–422 (2015).
4. Wang, X., Rohrer, G. S. & Li, H. Piezotronic modulations in electro- and photochemical catalysis. *MRS Bull.* **43**, 946–951 (2018).
5. Starr, M. B., Shi, J. & Wang, X. Piezopotential-driven redox reactions at the surface of piezoelectric materials. *Angew. Chemie - Int. Ed.* **51**, 5962–5966 (2012).
6. Anton, S. R. & Sodano, H. A. A review of power harvesting using piezoelectric materials (2003-2006). *Smart Mater. Struct.* **16**, (2007).
7. Li, J. *et al.* High Performance Piezoelectric Nanogenerators Based on Electrospun ZnO Nanorods/Poly(vinylidene fluoride) Composite Membranes. *J. Phys. Chem. C* **123**,

11378–11387 (2019).

8. Feng, W. *et al.* Atomically thin ZnS nanosheets: Facile synthesis and superior piezocatalytic H2 production from pure H2O. *Appl. Catal. B Environ.* **277**, 119250 (2020).
9. Sharma, A., Bhardwaj, U. & Kushwaha, H. S. ZnO hollow pitchfork: coupled photo-piezocatalytic mechanism for antibiotic and pesticide elimination. *Catal. Sci. Technol.* **12**, 812–822 (2022).
10. Ma, J. *et al.* High efficiency bi-harvesting light/vibration energy using piezoelectric zinc oxide nanorods for dye decomposition. *Nano Energy* **62**, 376–383 (2019).
11. Lan, S. *et al.* Performance and Mechanism of Piezo-Catalytic Degradation of 4-Chlorophenol: Finding of Effective Piezo-Dechlorination. *Environ. Sci. Technol.* **51**, 6560–6569 (2017).
12. Li, Y. *et al.* KNbO3/ZnO heterojunction harvesting ultrasonic mechanical energy and solar energy to efficiently degrade methyl orange. *Ultrason. Sonochem.* **78**, (2021).
13. Wang, Z. *et al.* Self-assembled NaNbO3-Nb2O5 (ferroelectric-semiconductor) heterostructures grown on LaAlO3 substrates. *Appl. Phys. Lett.* **101**, 0–4 (2012).
14. Kumar, D., Sharma, S. & Khare, N. Piezo-phototronic and plasmonic effect coupled Ag-NaNbO3 nanocomposite for enhanced photocatalytic and photoelectrochemical water splitting activity. *Renew. Energy* **163**, 1569–1579 (2021).
15. Wang, J., Hu, C., Zhang, Y. & Huang, H. Engineering piezoelectricity and strain sensitivity in CdS to promote piezocatalytic hydrogen evolution. *Chinese J. Catal.* **43**, 1277–1285 (2022).
16. Cui, H., Zhang, X. & Chen, D. Borophene: a promising adsorbent material with strong

ability and capacity for SO2 adsorption. *Appl. Phys. A Mater. Sci. Process.* **124**, 0 (2018).

17. Wu, W. *et al.* Piezoelectricity of single-atomic-layer MoS2 for energy conversion and piezotronics. *Nature* **514**, 470–474 (2014).
18. Balandin, A. A. Thermal properties of graphene and nanostructured carbon materials. *Nat. Mater.* **10**, 569–581 (2011).
19. Dai, H., Xiao, P. & Lou, Q. Application of SnO 2/MWCNTs nanocomposite for SF 6 decomposition gas sensor. *Phys. Status Solidi Appl. Mater. Sci.* **208**, 1714–1717 (2011).
20. Dauber, J. *et al.* Ultra-sensitive Hall sensors based on graphene encapsulated in hexagonal boron nitride. *Appl. Phys. Lett.* **106**, 1–5 (2015).
21. Zhang, S. *et al.* Recent progress in 2D group-VA semiconductors: From theory to experiment. *Chem. Soc. Rev.* **47**, 982–1021 (2018).
22. Piazza, Z. A. *et al.* Planar hexagonal B 36 as a potential basis for extended single-atom layer boron sheets. *Nat. Commun.* **5**, (2014).
23. Xie, S. Y., Wang, Y. & Li, X. Bin. Flat Boron: A New Cousin of Graphene. *Adv. Mater.* **31**, 1–13 (2019).
24. Mannix, A. J. *et al.* Synthesis of borophenes: Anisotropic, two-dimensional boron polymorphs. *Science (80-.).* **350**, 1513–1516 (2015).
25. Feng, B. *et al.* Experimental realization of two-dimensional boron sheets. *Nat. Chem.* **8**, 563–568 (2016).
26. Mannix, A. J., Zhang, Z., Guisinger, N. P., Yakobson, B. I. & Hersam, M. C. Borophene as a prototype for synthetic 2D materials development. *Nat. Nanotechnol.* **13**, 444–450 (2018).
27. Jiao, Y., Ma, F., Bell, J., Bilic, A. & Du, A. Two-Dimensional Boron Hydride Sheets:

High Stability, Massless Dirac Fermions, and Excellent Mechanical Properties. *Angew. Chemie* **128**, 10448–10451 (2016).

28. Kondo, T. Recent progress in boron nanomaterials. *Sci. Technol. Adv. Mater.* **18**, 780–804 (2017).
29. Zhang, Z., Penev, E. S. & Yakobson, B. I. Two-dimensional boron: Structures, properties and applications. *Chem. Soc. Rev.* **46**, 6746–6763 (2017).
30. Deng, D. *et al.* Catalysis with two-dimensional materials and their heterostructures. *Nat. Nanotechnol.* **11**, 218–230 (2016).
31. Zhang, X. *et al.* Boron Nanosheet: An Elemental Two-Dimensional (2D) Material for Ambient Electrocatalytic N2-to-NH3 Fixation in Neutral Media. *ACS Catal.* **9**, 4609–4615 (2019).
32. Chen, Y. *et al.* Highly Active, Nonprecious Electrocatalyst Comprising Borophene Subunits for the Hydrogen Evolution Reaction. *J. Am. Chem. Soc.* **139**, 12370–12373 (2017).
33. Marcano, D. C. *et al.* VOL. 4 ▪ NO. 8 ▪ 4806–4814 ▪ 2010.pdf. *ACS Nano* **4**, 4806–4814 (2010).
34. Sharma, A., Bhardwaj, U. & Kushwaha, H. S. Efficacious visible-light photocatalytic degradation of toxics by using Sr2TiMnO6-rGO composite for the wastewater treatment. *Clean. Eng. Technol.* **2**, 100087 (2021).
35. Ranjan, P. *et al.* Freestanding Borophene and Its Hybrids. *Adv. Mater.* **31**, (2019).
36. Ranjan, P. *et al.* A Low-Cost Non-explosive Synthesis of Graphene Oxide for Scalable Applications. *Sci. Rep.* **8**, 1–13 (2018).
37. Sharma, A., Bhardwaj, U. & Kushwaha, H. S. Ba2TiMnO6two-dimensional nanosheets

for rhodamine B organic contaminant degradation using ultrasonic vibrations. *Mater. Adv.* **2**, 2649–2657 (2021).

38. Sharma, A., Bhardwaj, U., Jain, D. & Kushwaha, H. S. NaNbO 3 Nanorods : Photopiezocatalysts for Elevated Bacterial 2 Disinfection and Wastewater Treatment. (2022) doi:10.1021/acsomega.1c06109.

39. Rodriguez, B. J., Callahan, C., Kalinin, S. V & Proksch, R. Dual-frequency resonance-tracking atomic force microscopy. *Nanotechnology* **18**, 475504 (2007).

40. Kim, S., Seol, D., Lu, X., Alexe, M. & Kim, Y. Electrostatic-free piezoresponse force microscopy. *Sci. Rep.* **7**, 1–8 (2017).

41. Taşaltın, N., Güllülü, S. & Karakuş, S. Dual-role of β borophene nanosheets as highly effective antibacterial and antifungal agent. *Inorg. Chem. Commun.* **136**, (2022).

42. Ding, J., Zheng, H., Wang, S. & Ji, X. Hydrogenated borophene nanosheets based multifunctional quasi-solid-state electrolytes for lithium metal batteries. *J. Colloid Interface Sci.* **615**, 79–86 (2022).

43. Xu, T. T. *et al.* Crystalline boron nanoribbons: Synthesis and characterization. *Nano Lett.* **4**, 963–968 (2004).

44. Li, H. *et al.* Scalable Production of Few-Layer Boron Sheets by Liquid-Phase Exfoliation and Their Superior Supercapacitive Performance. *ACS Nano* **12**, 1262–1272 (2018).

45. Ranjan, P., Lee, J. M., Kumar, P. & Vinu, A. Borophene: New Sensation in Flatland. *Adv. Mater.* **32**, 1–13 (2020).

46. Taşaltın, N. *et al.* Volatile organic compound detection performance of Borophene and PANI:β Borophene nanocomposite-based sensors. *J. Mater. Sci. Mater. Electron.* 24173–24181 (2022) doi:10.1007/s10854-022-09109-5.

47. Gruverman, A. P iezoresponse Force Microscopy : Electromechanical Behavior at the Nanoscale. **34**, (2017).

48. Tang, Q. *et al.* Enhanced Piezocatalytic Performance of BaTiO3 Nanosheets with Highly Exposed {001} Facets. *Adv. Funct. Mater.* **32**, (2022).

49. Lin, E. *et al.* BaTiO3 Nanosheets and Caps Grown on TiO2 Nanorod Arrays as Thin-Film Catalysts for Piezocatalytic Applications. *ACS Appl. Mater. Interfaces* **12**, 14005–14015 (2020).

50. Sharma, A., Bhardwaj, U., Jain, D. & Kushwaha, H. S. NaNbO 3 Nanorods : Photopiezocatalysts for Elevated Bacterial Disinfection and Wastewater Treatment. (2022) doi:10.1021/acsomega.1c06109.

51. Kamat, P. V., Huehn, R. & Nicolaescu, R. A 'sense and shoot' approach for photocatalytic degradation of organic contaminants in water. *J. Phys. Chem. B* **106**, 788–794 (2002).

52. Ma, J. *et al.* Pyroelectric Pb(Zr 0.52 Ti 0.48)O 3 polarized ceramic with strong pyro-driven catalysis for dye wastewater decomposition. *Ceram. Int.* **45**, 11934–11938 (2019).

53. Wu, J. *et al.* Strong pyro-catalysis of pyroelectric BiFeO3 nanoparticles under a room-temperature cold-hot alternation. *Nanoscale* **8**, 7343–7350 (2016).

54. Wu, J., Qin, N. & Bao, D. Effective enhancement of piezocatalytic activity of BaTiO3 nanowires under ultrasonic vibration. *Nano Energy* **45**, 44–51 (2018).

55. Singh, G., Sharma, M. & Vaish, R. Transparent ferroelectric glass–ceramics for wastewater treatment by piezocatalysis. *Commun. Mater.* **1**, (2020).

56. Tezcanli-Güyer, G. & Ince, N. H. Individual and combined effects of ultrasound, ozone and UV irradiation: A case study with textile dyes. *Ultrasonics* **42**, 603–609 (2004).

57. Ghows, N. & Entezari, M. H. Kinetic investigation on sono-degradation of Reactive Black

5 with core-shell nanocrystal. *Ultrason. Sonochem.* **20**, 386–394 (2013).

58. Copie, O. *et al.* Adsorbate Screening of Surface Charge of Microscopic Ferroelectric Domains in Sol-Gel PbZr0.2Ti0.8O3 Thin Films. *ACS Appl. Mater. Interfaces* **9**, 29311–29317 (2017).

59. Lei, H. *et al.* Piezoelectric polarization promoted spatial separation of photoexcited electrons and holes in two-dimensional g-C3N4 nanosheets for efficient elimination of chlorophenols. *J. Hazard. Mater.* **421**, 126696 (2022).

60. Zi, Y. *et al.* Triboelectric-pyroelectric-piezoelectric hybrid cell for high-efficiency energy-harvesting and self-powered sensing. *Adv. Mater.* **27**, 2340–2347 (2015).

List of figures

Fig.1 (a) XRD pattern of the prepared borophene sheets (b) Raman spectrum of the borophene nanosheets, (c) FTIR spectrum of borophene nanosheets, (d-e) Binding energy spectra of B 1s before and after reaction

Fig.2: (a and c) HR HAADF images of the borophene nanosheets, (b) SAED pattern of the nanosheets, (d-e) AFM images of the borophene nanosheets

Fig.3: (a) AFM morphology, (b) amplitude OP-PFM, (c) amplitude IP-PFM images simultaneously recorded on the borophene surface, and (d) characteristic amplitude piezoresponse loop recorded on borophene nanosheets

Fig.4: (a) Formation of piezo potential, (b) piezo current response.

Fig.5: Piezocatalytic degradation of (a) rose bengal, (b) Methylene blue, (c) Mixture of dyes, (d) Overall decomposition ratio of different pollutants, (e) Degradation efficiency of the borophene with different pollutants, (f) kinetic order curve

Fig.6: (a) Photoluminescence spectra for the detection of $OH^{\cdot}$ radicals by using terephthalic acid, (b) Degradation of nitroblue tetrazolium (NBT) under the piezocatalytic effect to confirm the generation of super oxide radical ($\bullet O_2^-$)

Fig.7: Proposed mechanism of piezocatalysis

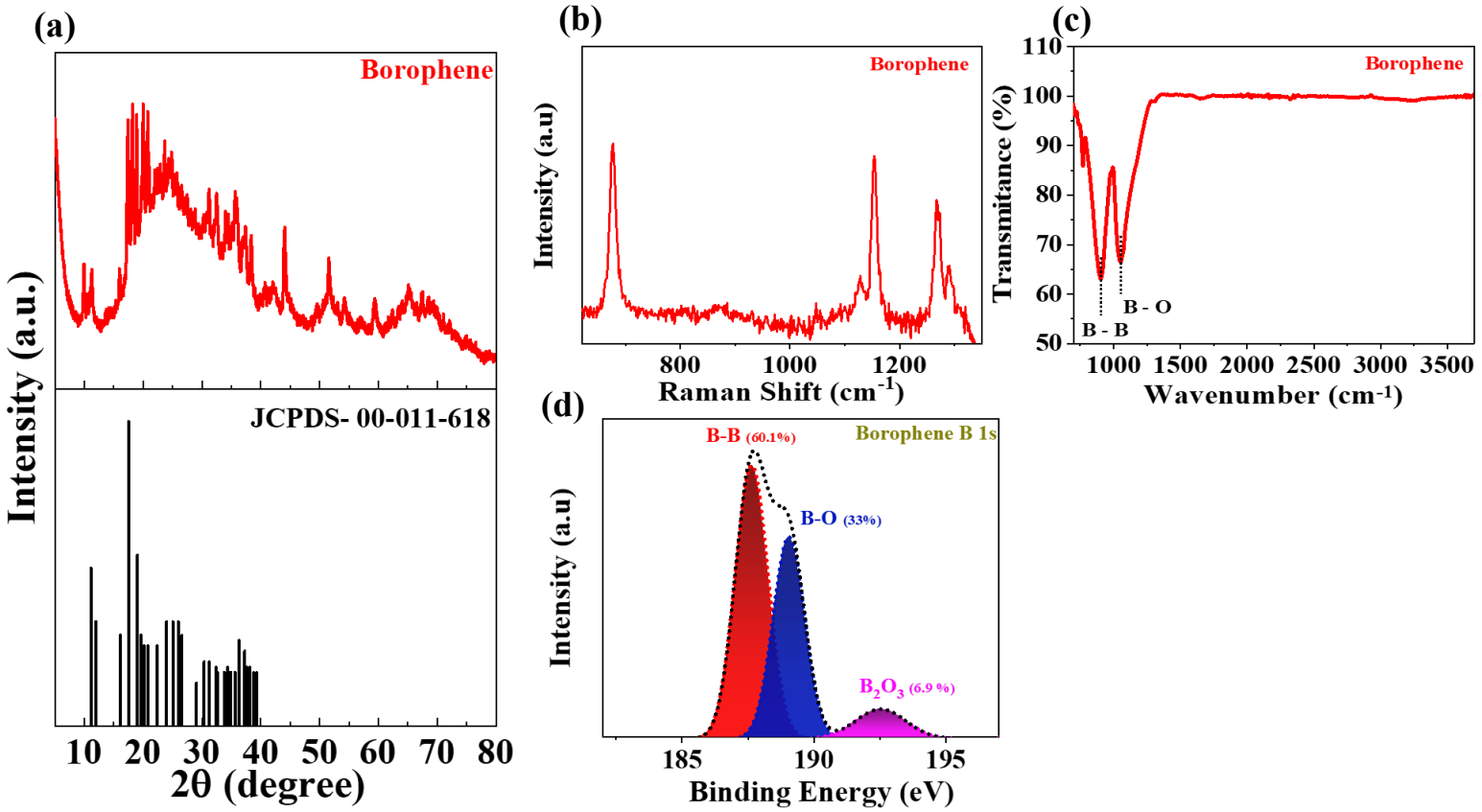
(a)
Borophene
JCPDS- 00-011-618
Intensity (a.u.)
10 20 30 40 50 60 70 80
2θ (degree)
(b)
Borophene
Intensity (a.u)
800 1000 1200
Raman Shift (cm-1)
(c)
Borophene
Transmitance (%)
110 100 90 80 70 60 50
B - B
B - O
1000 1500 2000 2500 3000 3500
Wavenumber (cm-1)
(d)
B-B (60.1%)
Borophene B 1s
B-O (33%)
B2O3 (6.9 %)
Intensity (a.u)
185 190 195
Binding Energy (eV)

Fig. 1

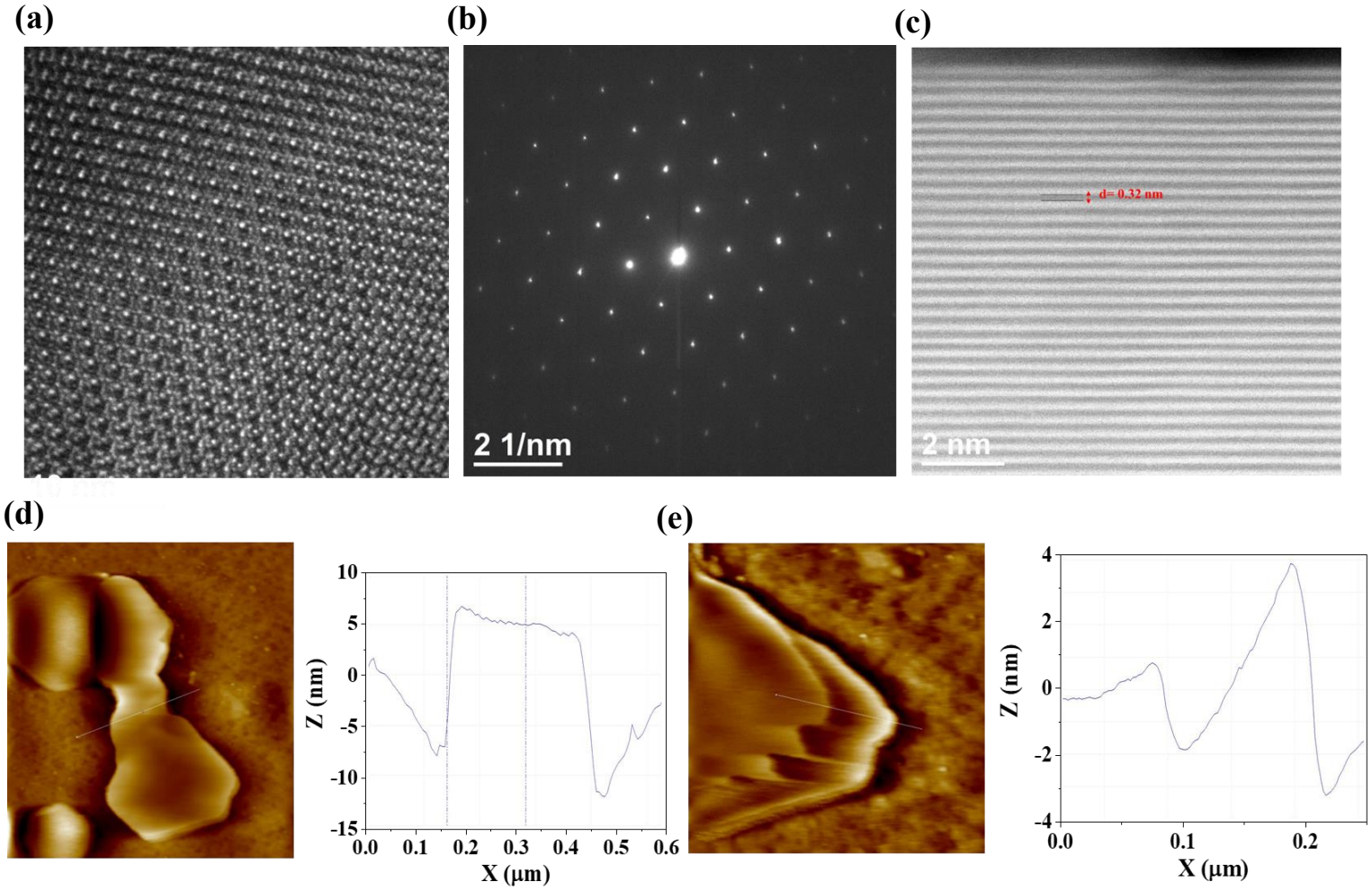

Fig. 2

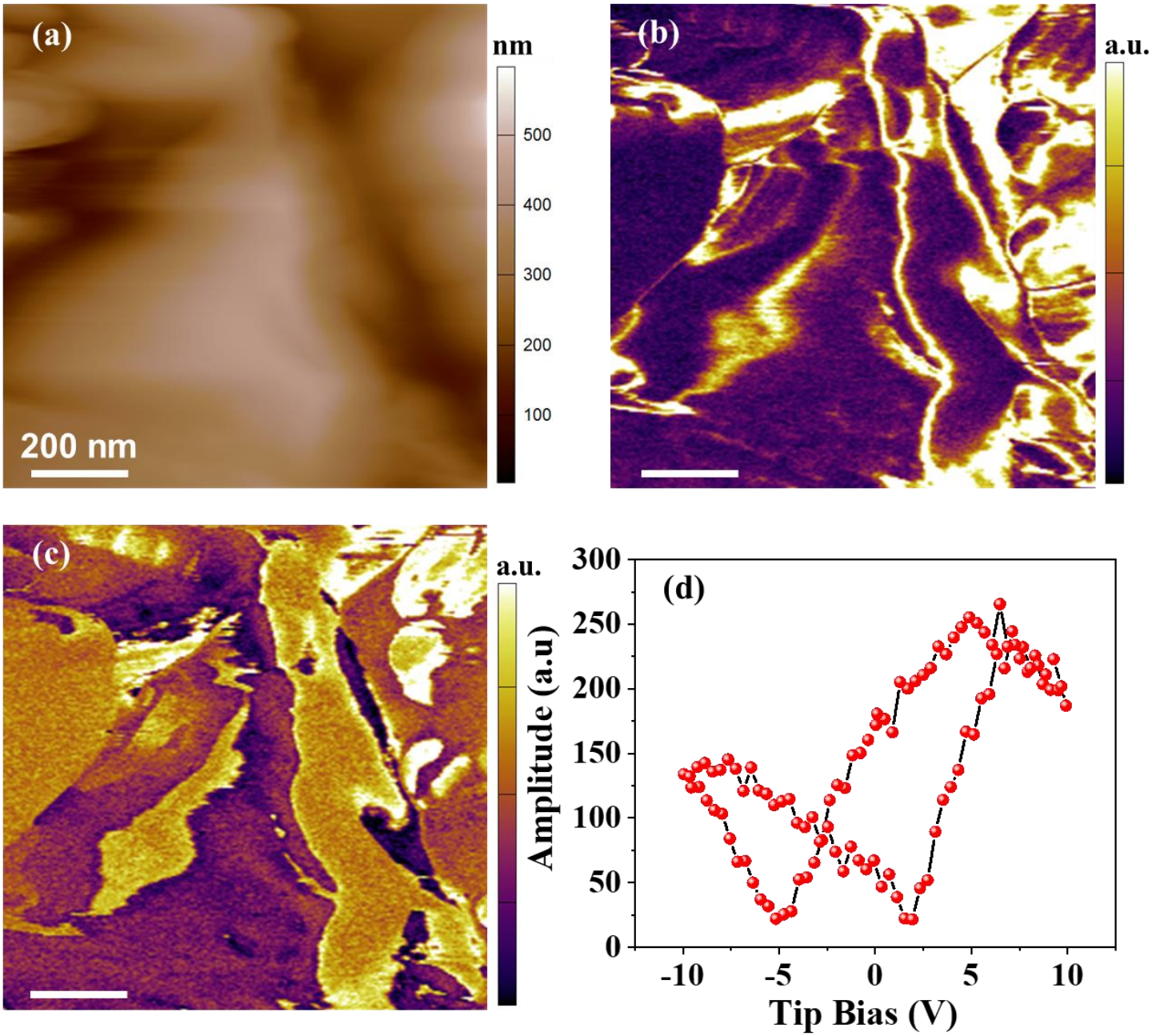
(a)
nm
500
400
300
200
100
200 nm
(b)
a.u.
(c)
a.u.
(d)
Amplitude (a.u)
300
250
200
150
100
50
0
-10
-5
0
5
10
Tip Bias (V)

Fig. 3

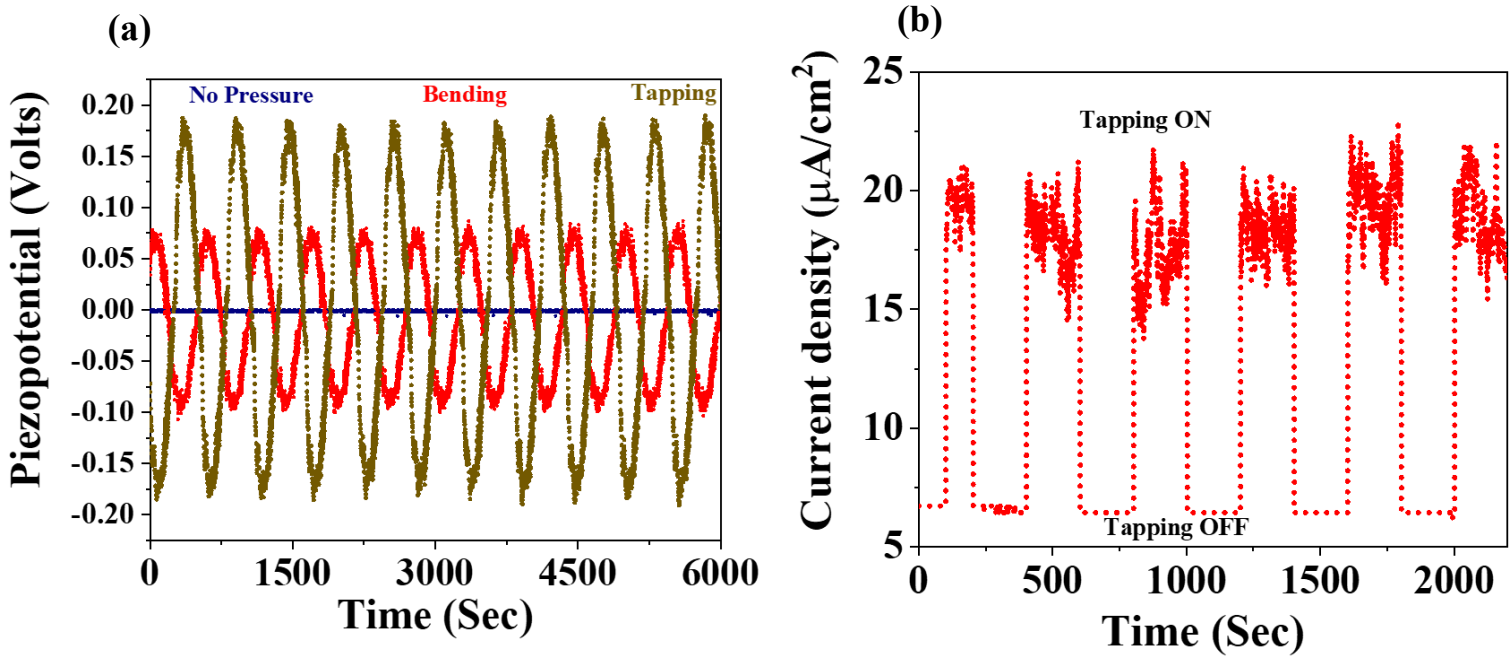
(a)
No Pressure
Bending
Tapping
Piezopotential (Volts)
0.20
0.15
0.10
0.05
0.00
-0.05
-0.10
-0.15
-0.20
0
1500
3000
4500
6000
Time (Sec)
(b)
Tapping ON
Tapping OFF
Current density (μA/cm2)
25
20
15
10
5
0
500
1000
1500
2000
Time (Sec)

Fig. 4

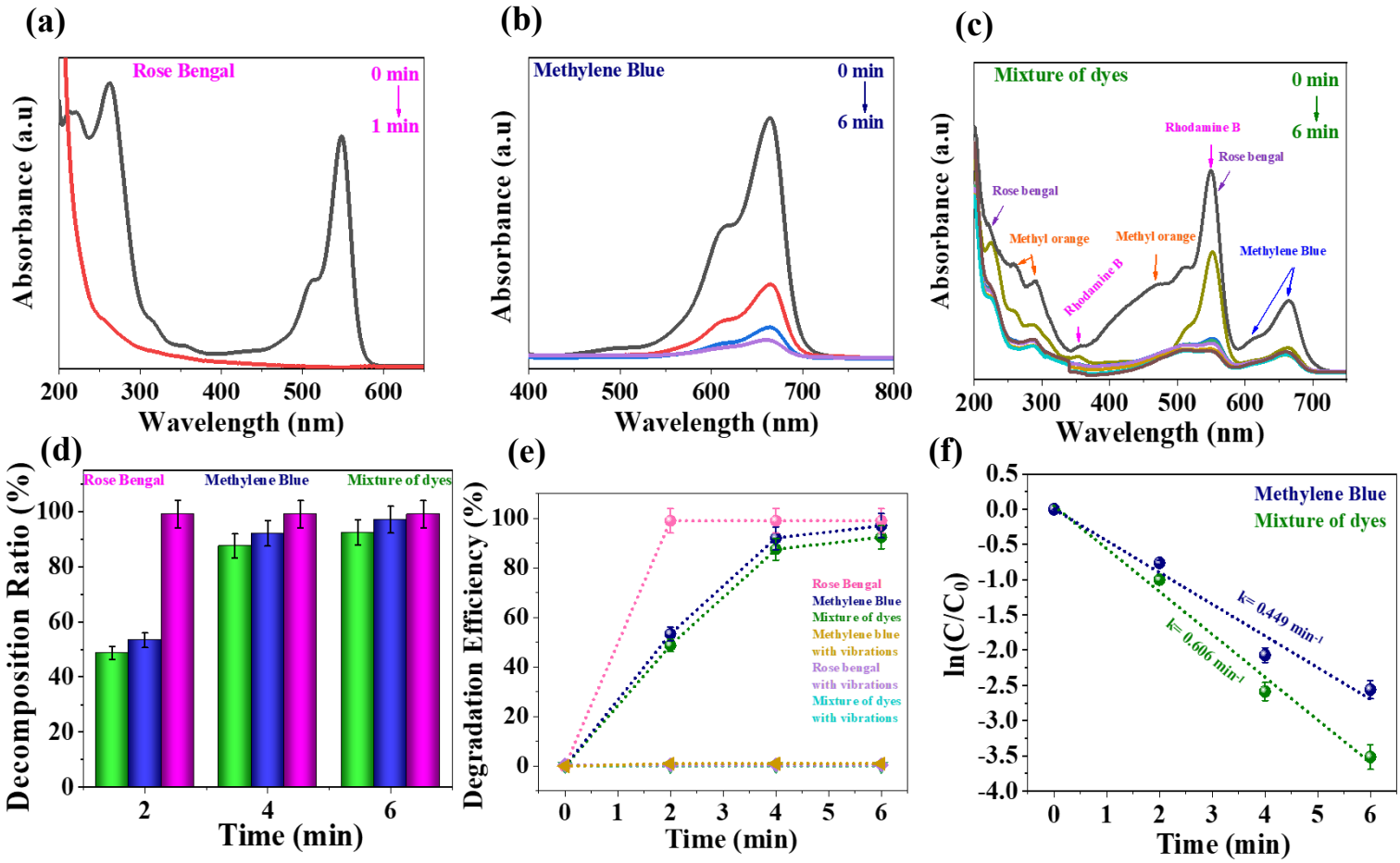
(a)
Rose Bengal
0 min
1 min
Absorbance (a.u)
Wavelength (nm)
(b)
Methylene Blue
0 min
6 min
Absorbance (a.u)
Wavelength (nm)
(c)
Mixture of dyes
0 min
6 min
Rhodamine B
Rose bengal
Rose bengal
Methyl orange
Methyl orange
Rhodamine B
Methylene Blue
Absorbance (a.u)
Wavelength (nm)
(d)
Rose Bengal
Methylene Blue
Mixture of dyes
Decomposition Ratio (%)
Time (min)
(e)
Rose Bengal
Methylene Blue
Mixture of dyes
Methylene blue with vibrations
Rose bengal with vibrations
Mixture of dyes with vibrations
Degradation Efficiency (%)
Time (min)
(f)
Methylene Blue
Mixture of dyes
k= 0.449 min-1
k= 0.606 min-1
ln(C/C0)
Time (min)

Fig. 5

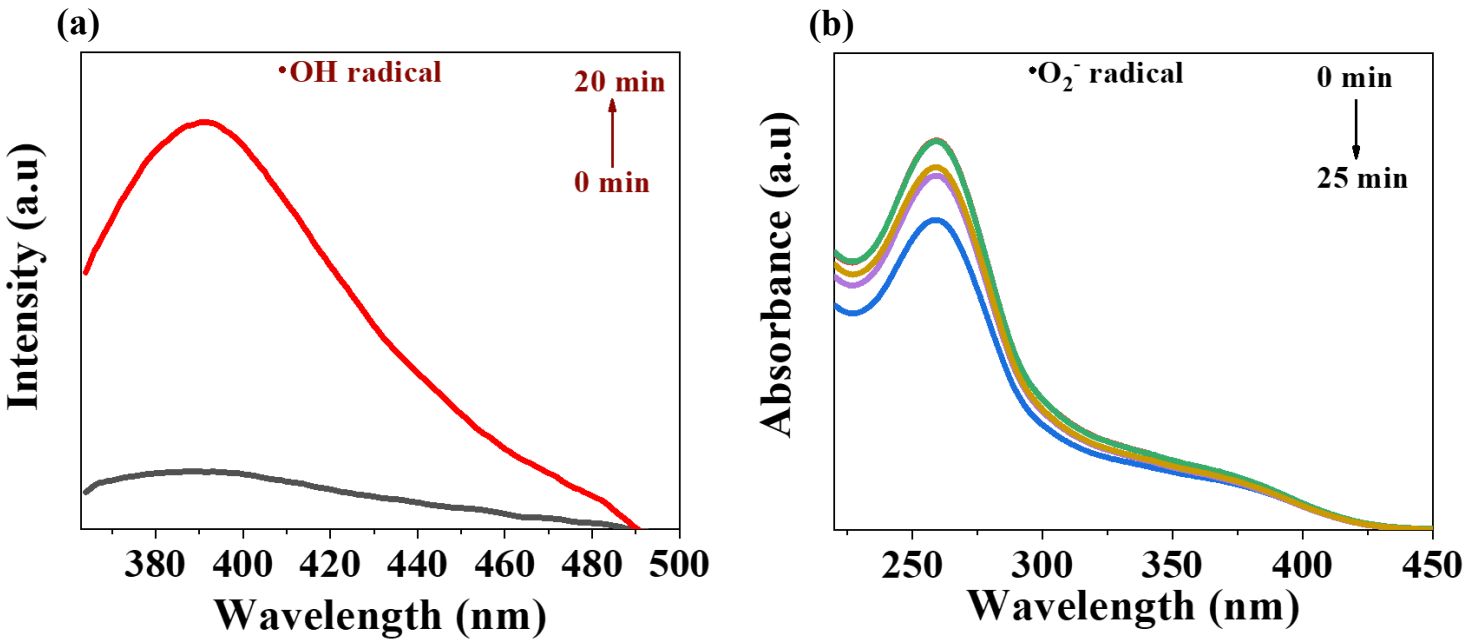
(a)
•OH radical
20 min
0 min
Intensity (a.u)
380
400
420
440
460
480
500
Wavelength (nm)
(b)
•O2- radical
0 min
25 min
Absorbance (a.u)
250
300
350
400
450
Wavelength (nm)

Fig. 6

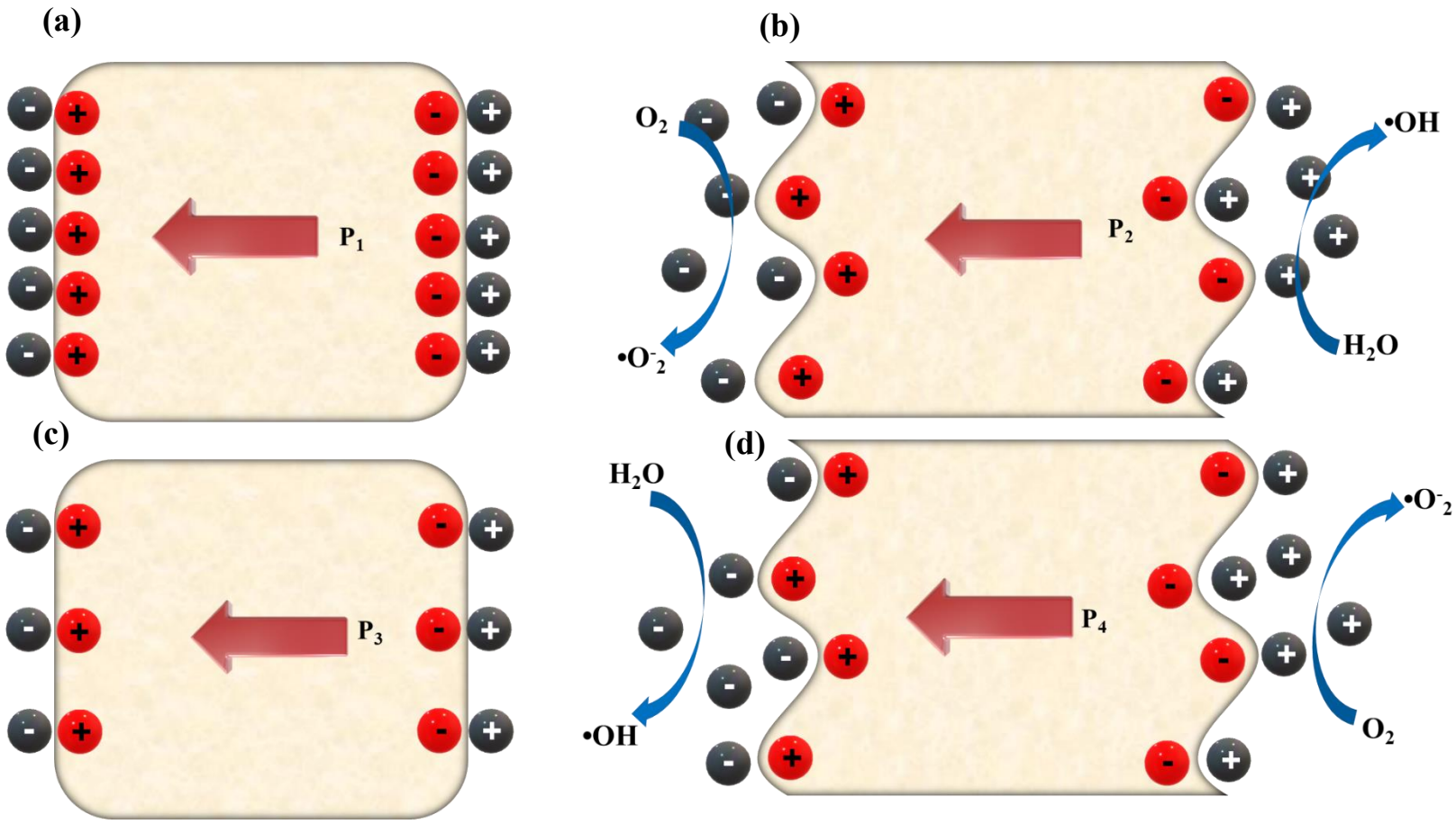

Fig. 7

Table S1- comparison of different piezocatalytic systems

Piezocatalysts	Pollutants	Reaction time (minutes)	Degradation Efficiency (%)	References
Ba_2TiMnO_6	Rhodamine B (5 mg/L)	180	99	[39]
Bi_2WO_6	Methylene Blue (10 mg/L)	35	96	[55]
ZnO nanorods	AO7 (10 mg/L)	100	32	[56]
$BaTiO_3$ nanowires	Methyl Orange (5mg/L)	160	90	[57]
$NaNbO_3$ nanorods	Methylene Blue (0.01 mM)	190	19	[58]
$BiFeO_3$ nanowires	Rhodamine B (4 mg/L)	60	60	[59]
$LuFeO_3$ nanoparticles	Rhodamine B (5 mg/L)	90	30	[61]
$NaNbO_3$ nanorods	Rhodamine B (10 mg/L)	80	75	[62]
Borophene nanosheets	**Methylene blue**	**6**	**97**	**This work**

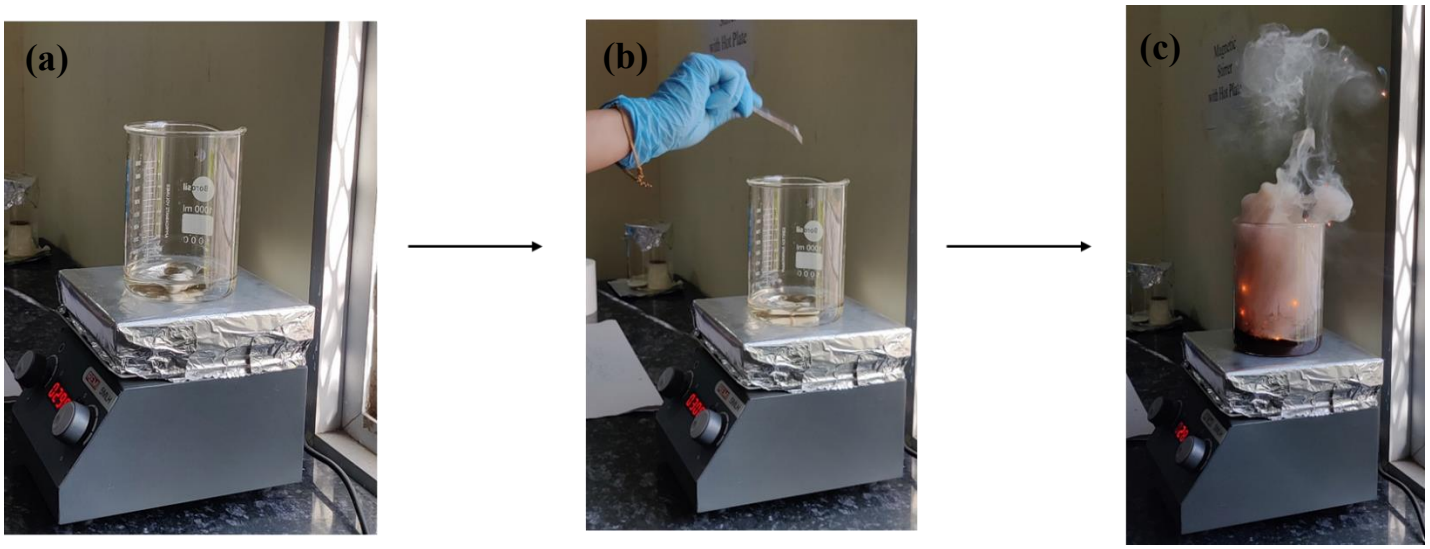

Figure S1- Synthesis of Borophene nanosheets.

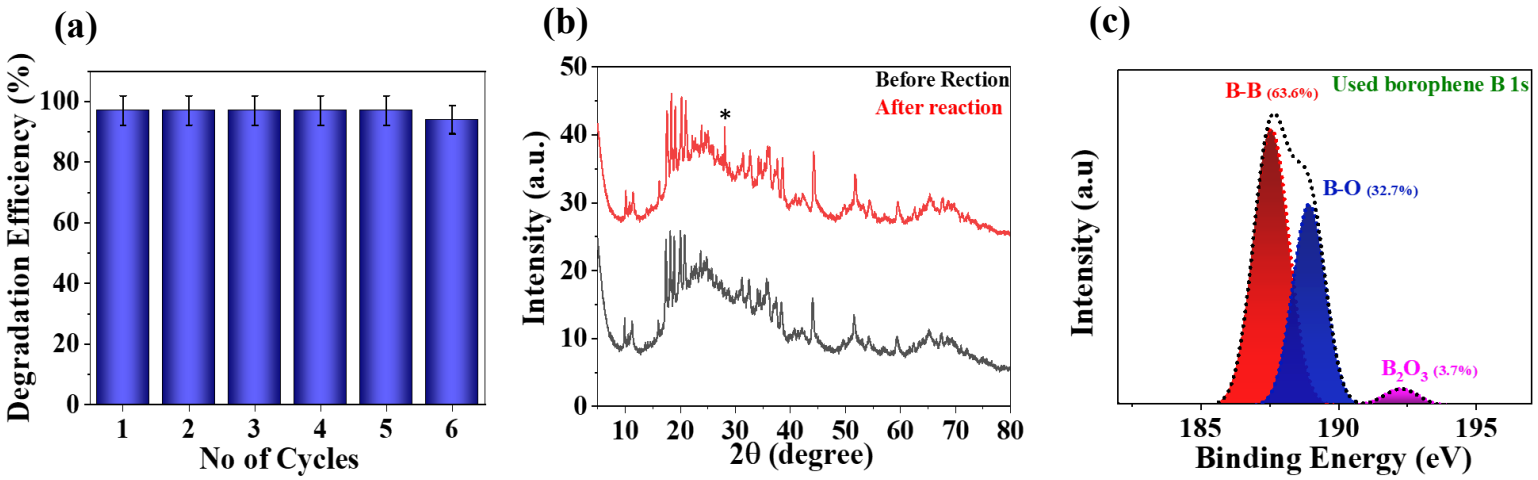

Figure S2- (a) Recyclability of borophene nanosheets, (b) XRD pattern of borophene before and after piezocatalysis (* = B_2O_3), (c) High resolution spectra of used borophene.